


Article

Synthesis, Structure, and UV–Vis Characterization of Antimony(III) Phthalocyanine: $[(\text{SbPc})_2(\text{Sb}_2\text{I}_8)(\text{SbBr}_3)]_2$

Ryszard Kubiak and Jan Janczak * 

Institute of Low Temperature and Structure Research, Polish Academy of Sciences, Okólna 2, 50-422 Wrocław, Poland; r.kubiak@intibs.pl

* Correspondence: j.janczak@intibs.pl

Abstract: A new antimony(III)–phthalocyanine complex with the formula of $[(\text{SbPc})_2(\text{Sb}_2\text{I}_8)(\text{SbBr}_3)]_2$ has been obtained in the reaction of pure antimony powder with phthalonitrile under the oxidation conditions by iodine monobromide vapors. The complex crystallizes in the centrosymmetric space group of the triclinic system. Both independent $(\text{SbPc})^+$ units exhibit non-planar conformation, since the Sb(III) is larger than the equilibrium cavity size of the ring and cannot be accommodated without its expansion; thus, the metal protrudes out of the cavity, forming a saucer shape. The centrosymmetric anionic unit of the crystal consists of two $(\text{Sb}_2\text{I}_8)^{2-}$ interacted anionic units forming $(\text{Sb}_6\text{I}_{16})^{4-}$ anionic complex that interacts with two SbBr_3 molecules to form $[\text{Sb}_6\text{I}_{16}\text{Br}_6]^{4-}$ anionic aggregate. Each $[\text{Sb}_6\text{I}_{16}\text{Br}_6]^{4-}$ anionic aggregate is surrounded by four $(\text{SbPc})^+$ cations forming a supramolecular centrosymmetric $(\text{SbPc})_4[\text{Sb}_6\text{I}_{16}\text{Br}_6]$ complex. Translationally related $(\text{SbPc})_4[\text{Sb}_6\text{I}_{16}\text{Br}_6]$ molecules form a stacking structure along the [100] and [011] directions with $\text{N}_4\text{--N}_4$ distances of 3.55 and 3.53 Å, respectively, between the back-to-back-oriented saucer-shaped $(\text{SbPc})^+$ units. The interaction between the building units of the crystal was analyzed using the Hirshfeld surface and the analysis of the 2D fingerprint plots. The UV–Vis absorption spectra of crystal **1** were taken in CH_2Cl_2 and toluene solutions in the concentration range from 10^{-5} to 10^{-6} mol/L. No significant changes related to aggregation in solutions were observed. The Q-band in toluene solution is red shifted by ~15 nm in comparison to that in CH_2Cl_2 solution. Oxidation of $(\text{SbPc})_4[\text{Sb}_6\text{I}_{16}\text{Br}_6]$ yields $\text{Sb}^{\text{V}}\text{Pc}$ derivative. Both Sb^{III} and Sb^{V} phthalocyanine derivatives absorb near infrared light (600–900 nm), which should be intriguing from the point of view of potential use as photosensitizers for PDT and as an infrared cut filter for plasma display and silicon photodiodes.

Keywords: antimony(III) phthalocyanine; crystal structure; Hirshfeld surface; oxidation; UV–Vis spectroscopy



Citation: Kubiak, R.; Janczak, J. Synthesis, Structure, and UV–Vis Characterization of Antimony(III) Phthalocyanine:

$[(\text{SbPc})_2(\text{Sb}_2\text{I}_8)(\text{SbBr}_3)]_2$. *Molecules* **2022**, *27*, 1839. <https://doi.org/10.3390/molecules27061839>

Academic Editor: Igor Djerdj

Received: 21 January 2022

Accepted: 5 March 2022

Published: 11 March 2022

Publisher's Note: MDPI stays neutral with regard to jurisdictional claims in published maps and institutional affiliations.

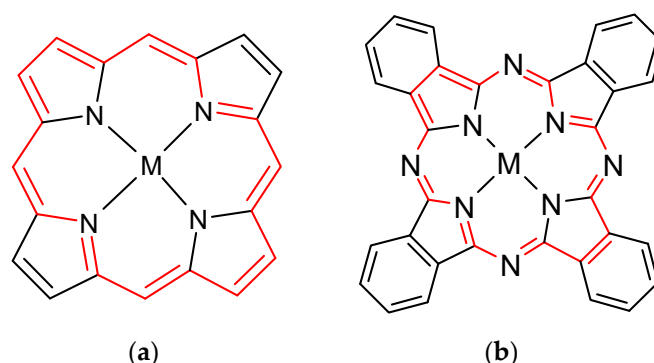


Copyright: © 2022 by the authors. Licensee MDPI, Basel, Switzerland. This article is an open access article distributed under the terms and conditions of the Creative Commons Attribution (CC BY) license (<https://creativecommons.org/licenses/by/4.0/>).

1. Introduction

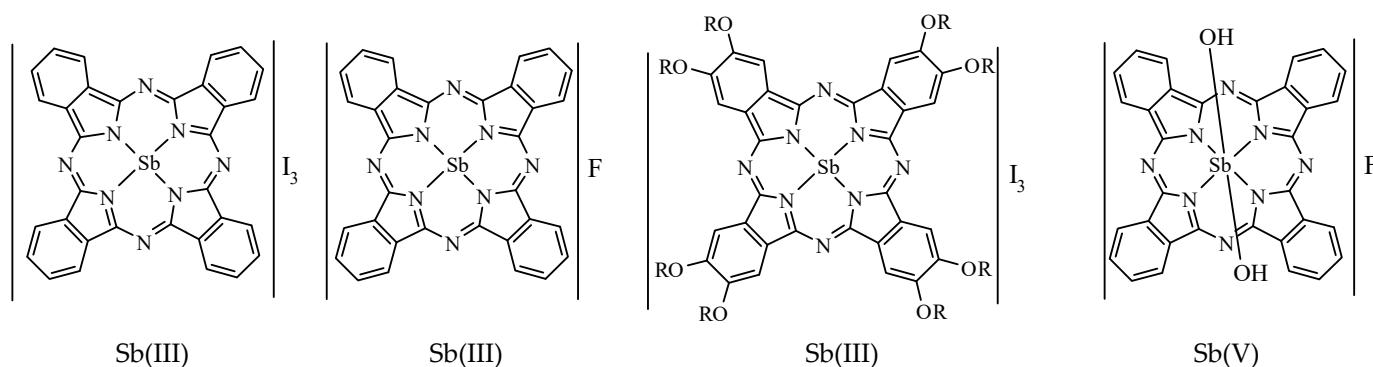
Phthalocyanine and its metal complexes are still very intensively studied due to their various technological applications. The initial interest in them resulted from their deep and intense color; hence, they were used as pigments in the plastic industry and as dyes in the textile industry [1–9]. The dyeing properties of metallophthalocyanines result from their structure and very strong characteristic optical absorption in the visible region, the so-called Q band, which is characteristic for a macrocyclic tetrapyrrole ring with an 18π -electron-conjugated tetrapyrrole macrocycles (Scheme 1) [10]. The molar extinction coefficient of the Q-band of metal-free porphyrin, is $1.71 \times 10^5 \text{ dm}^3 \cdot \text{mol}^{-1} \cdot \text{cm}^{-1}$ at 407 nm, and for metal-free phthalocyanine it is $2.766 \times 10^5 \text{ dm}^3 \cdot \text{mol}^{-1} \cdot \text{cm}^{-1}$ in the visible spectral region (669 nm), and they may vary significantly depending on the solvents [11]. For metalloporphyrins and metallophthalocyanines, the molar extinction coefficient varies depending on the central metal as well as on the solvent in the wide range, for example, for the zinc porphyrin and zinc phthalocyanine the molar extinction coefficient is $5.74 \times 10^5 \text{ dm}^3 \cdot \text{mol}^{-1} \cdot \text{cm}^{-1}$ at 422.8 nm and $2.818 \times 10^5 \text{ dm}^3 \cdot \text{mol}^{-1} \cdot \text{cm}^{-1}$ at 674 nm, respectively [12,13]. The molar

extinction coefficients of several metal(II) phthalocyanines in various solvents derived from the intensities of the Q-band were recently published [14].



Scheme 1. Metalloporphyrins (a) and metallophthalocyanines (b) showing the 18 π -electron tetrapyrrole macrocycle (in red). For metal-free porphyrin or metal-free phthalocyanine, M is two hydrogens.

For antimony(III)-phthalocyanine derivatives (Scheme 2) in ethanol solution, the molar extinction coefficient is 1.059×10^5 and 1.717×10^5 $\text{dm}^3 \cdot \text{mol}^{-1} \cdot \text{cm}^{-1}$ at ~ 730 nm for unsubstituted Sb(III) phthalocyanine and 1.06×10^5 $\text{dm}^3 \cdot \text{mol}^{-1} \cdot \text{cm}^{-1}$ at ~ 740 nm for octa-substituted Sb(III) phthalocyanine, whereas for Sb(V) phthalocyanine, the molar extinction coefficient is 1.908×10^5 $\text{dm}^3 \cdot \text{mol}^{-1} \cdot \text{cm}^{-1}$ at 699 nm [15,16].



Scheme 2. Examples of some Sb(III) and Sb(V) phthalocyanines (-OR = $\text{C}_6\text{H}_5\text{O}$ - or *tert*-butylO-).

Further interest of metallophthalocyanines results from their interesting properties, such as electronic, photonic, and photovoltaic that have already found industrial applications in many instruments or chemical processes, including catalysis, gas sensors, solar cells, charge-generating materials, optical data storage, infrared cut-off filters, active matrix displays, light organic-emitting diodes (OLED), organic photovoltaics (OPVs), etc. [17–27]. Strong and intense absorption of light by metal phthalocyanines in the so-called therapeutic window, namely in the near-infrared (NIR) region of visible light (600–900 nm), proved to be promising for photodynamic cancer therapy (PDT) in which they can be used as photosensitizers [28–35].

The physical and chemical properties of metallophthalocyanines are varied by the structure of the macrocyclic ligand with the extended π -electron delocalization system as well as by the central metal. Planar metallophthalocyanines with 18 π electrons conjugate form a stacking structure in the solid state stabilized by π - π interactions, and this limits their solubility in the most commonly used organic solvents and undergo molecular aggregation [36]. Aggregation phenomena are common in chemistry of phthalocyanines and are known to give rise to significant changes in their physical properties [37–39] and may arouse interest from the point of view of supramolecular chemistry [40]. Metallophthalocyanines containing heavy atoms with too large radii to fit into the phthalocyanine core

are nonplanar and lead to the reduction of π - π interactions and improve the intersystem crossing [41], resulting in the improvement in photophysical and photochemical properties as well as improve their solubility due to the reduction of molecular aggregation, resulting from changes in the electronic structure of the molecule as well as due to the dipole moment of the non-planar molecule [42].

A large number of metallophthalocyanine derivatives have so far been studied; however, the metallophthalocyanines with group 15 elements, unlike porphyrins analogues [43–47], were ignored for a long time until the first derivatives of bismuth and antimony were identified [48–51], and their structural characterizations are still less explored [52–64]. The variable valency of these metals depending on the reaction conditions (III or V) can lead to the formation of various MPc derivatives. SbPc derivatives can be promising candidates for new drugs because they are stable, powerful electron donors/acceptors [65,66], and some derivatives undergo facile $\text{Sb}^{\text{III}}/\text{Sb}^{\text{V}}$ conversion under mild conditions [67,68]. Their use as drugs requires further research on their biocompatibility and effectiveness as well as their toxicity.

In this work, we report synthesis and X-ray structural characterization of a novel antimony(III) phthalocyanine, $[(\text{Sb}^{\text{III}}\text{Pc})_2(\text{Sb}_2\text{I}_8)(\text{SbBr}_3)]$, obtained under an iodine monobromide vapor atmosphere. The Sb^{III} cation with a radius of about 0.90 Å [69] is larger than the size of the ring cavity and cannot be accommodated without ring expansion; therefore, the formation of non-planar derivatives of $\text{Sb}^{\text{III}}\text{Pc}$ can be expected. The antimony(III)-phthalocyanine complexes can be oxidized to $\text{Sb}^{\text{V}}\text{Pc}$ derivatives. In addition, the obtained antimony(III) phthalocyanine and its oxidized $\text{Sb}^{\text{V}}\text{Pc}$ derivative, as described below, exhibits absorption of a wide range of visible light. Therefore, this should be of interest to those who work not only with dyes and pigments but also with solar cells and charge-generating material. It should be noted that antimony-phthalocyanine derivatives due to strong absorption of light in the therapeutic window may be attractive from the viewpoint of their potential application as a photosensitizer for PDT [70–74].

2. Experimental Section

2.1. General Procedure

Phthalonitrile (98%), iodine monobromide (98%), and antimony (99.999%) were obtained from Merck (Darmstadt, Germany) and used as received. The composition of the obtained crystals was checked with energy dispersive spectroscopy (EDS) (FEI company, Thermo Fisher Scientific, Waltham, MA, USA). EDS spectra were acquired and analyzed using an EDAX Pegasus XM4 spectrometer with an SDD Apollo 4D detector mounted on a FEI Nova NanoSEM 230 microscope. In addition, the elemental analysis was also carried out with a PerkinElmer 240 elemental analyzer (Waltham, MA, USA). The Fourier transform infrared spectra were recorded between 4000 and 450 cm^{-1} on a Bruker IFS 113 V FTIR (Bruker Optik GmbH, Leipzig, Germany) in nujol mull (Figure S1, in Supplementary Materials). Measurements of the UV-Vis spectra were carried out at room temperature using an Agilent UV-Vis/NIR Cary 5000 spectrometer (Agilent Technologies, Inc., Santa Clara, CA, USA). The UV-Vis spectra were recorded in CH_2Cl_2 and toluene solutions with concentrations ranging from 1×10^{-5} to 1×10^{-6} mol/L.

2.2. Synthesis $[(\text{Sb}^{\text{III}}\text{Pc})_2(\text{Sb}_2\text{I}_8)(\text{SbBr}_3)]_2$

The crystals of the $[(\text{Sb}^{\text{III}}\text{Pc})_2(\text{Sb}_2\text{I}_8)(\text{SbBr}_3)]_2$ (1) were isolated as a product of the reaction of Sb (0.1218 g, 1.0 mmol) with phthalonitrile (0.51252 g, 4 mmol) under iodine monobromide vapor according to a slightly modified method described elsewhere [75]. The powder Sb and phthalonitrile (in a molar proportion of 1:4) were mixed with iodine monobromide (2.068 g, 10.0 mmol) and pressed into the pellets. The pellets were inserted into an evacuated glass ampoule and sealed. The ampoule was heated at 240 °C for one day, and next, it was cooled to room temperature. After such a process, good quality single crystals of $[(\text{Sb}^{\text{III}}\text{Pc})_2(\text{Sb}_2\text{I}_8)(\text{SbBr}_3)]$ suitable for the X-ray analysis were formed. Anal.

Found: C, 26.51; Br, 8.26; I, 35.21; N, 7.72, and Sb, 21.20%. Calc. for $C_{64}H_{32}Br_3I_8N_{16}Sb_5$: C, 26.61; Br, 8.30; I, 35.14; N, 7.76; Sb, 21.07; and H, 1.12%.

2.3. X-ray Crystallography

X-ray intensity data collection for the $[(Sb^{III}Pc)_2(Sb_2I_8)(SbBr_3)]-(1)$ crystal was collected using graphite monochromatic $MoK\alpha$ radiation on a four-circle κ geometry Xcalibur diffractometer with Sapphire2 area CCD detector. Data collections were made using the CrysAlis CCD program [76]. Integration, scaling of the reflections, correction for Lorenz and polarization effects, and absorption corrections were performed using the CrysAlis Red program [76]. The structures were solved by the direct methods using SHELXT-2014/7 [77] and refined using the SHELXL-2018/3 program [78]. The hydrogen atoms joined to aromatic carbon atoms were introduced in their geometrical positions and treated as rigid. The final difference Fourier maps showed no peaks of chemical significance. Details of the data collection parameters, crystallographic data, and final agreement parameters are collected in Table 1. Visualizations of the structures were made with the Diamond 3.0 [79].

Table 1. Crystal data and final refinement parameters for 1.

	$[(Sb^{III}Pc)_2(Sb_2I_8)(SbBr_3)]-(1)$
Formula	$C_{64}H_{32}Br_3I_8N_{16}Sb_5$
Molecular weight	2888.73
Temperature (K)	295(2)
Crystal system	Triclinic
Space group	$P\bar{1}$
a, b, c (Å)	14.399(2), 15.344(3), 18.992(3)
α, β, γ (°)	95.64(2), 96.89(2), 113.93(2)
V (Å ³)	3757.4(12)
Z	2
D_{cal} (g cm ⁻³)	2.553
Crystal size (mm ³)	0.250 × 0.125 × 0.080
μ (mm ⁻¹)	6.707
Absorption correction	multi-scan
T_{max}/T_{min}	0.4754/1.000
Total/Unique/Obs refts	23,647/14,738/7721
R_{int}	0.0271
$R, [F^2 > 2\sigma(F^2)]^1$	0.0476
$wR [F^2 \text{ all refts}]^2$	0.0957
S	1.001
$\Delta\rho_{max}, \Delta\rho_{min}$ (e·Å ⁻³)	2.072, -1.286

¹ $R = \sum ||F_o| - |F_c|| / \sum F_o$; ² $wR = \{ \sum [w(F_o^2 - F_c^2)^2] / \sum wF_o^4 \}^{1/2}$; $w^{-1} = \sigma^2(F_o^2) + (aP)^2$ where $P = (F_o^2 + 2F_c^2)/3$. The a parameter is 0.0263.

2.4. Hirshfeld Surface Analysis

Hirshfeld surface analysis and 2D fingerprint plots as well as percentage contributions for various intermolecular contacts in the investigated crystals, were calculated using the Crystal Explorer Ver. 3.1 program package [80].

2.5. Theoretical Calculations

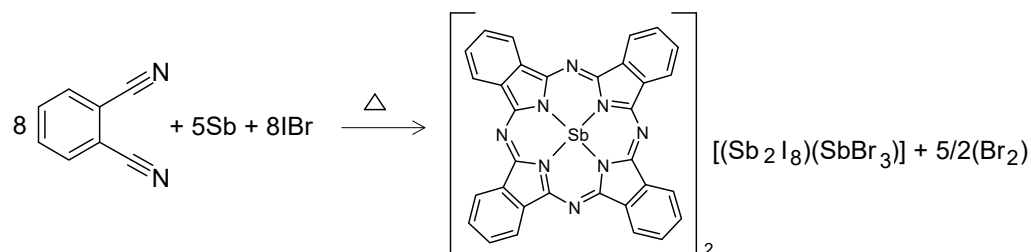
The optimized geometry of the $(SbPc)^+$ unit was performed based on the experimental X-ray geometry using the DFT and PBEPBE functional and LAN2MB basis sets using the Gaussian 2016 program package [81].

3. Results and Discussion

3.1. Synthesis and Initial Characterization

The preparation method leads directly to good-quality $[(Sb^{III}Pc)_2(Sb_2I_8)(SbBr_3)]-(1)$ single crystals. During prolonged heating, the liquid phthalonitrile undergoes catalytic tetramerization forming the phthalocyanine units while accepting the two electrons from

the antimony present in the reaction forming $(\text{Sb}^{\text{III}}\text{Pc})^+$ cationic units (Scheme 3). Simultaneously, the iodine monobromide accepted the third electron as well as oxidized the excess of antimony present in the reaction forming the centrosymmetric $\{[(\text{Sb}_2\text{I}_8)(\text{SbBr}_3)]_2\}^{4-}$ anionic complex. These oppositely charged units interact with each other, leading to nucleation and, over time, to crystallization and growth of good-quality single crystals suitable for X-ray diffraction.



Scheme 3. Synthesis of antimony phthalocyanine under oxidation condition of iodine monobromide vapor.

It should be noted that the heating time should not be extended too long, as it leads to partial decomposition of the phthalocyanine complex formed and to the formation of the phthalonitrile trimer [82]. Elemental analysis of the obtained crystals gave a satisfactory result, which is close to the calculated one. The sharp peak for the $\text{C}\equiv\text{N}$ stretching vibrations in the IR spectrum of phthalonitrile at $\sim 2200\text{ cm}^{-1}$ disappeared after tetramerization into phthalocyanine moiety [83,84]. The IR spectrum of $(\text{SbPc})(\text{I}_3)\frac{1}{2}(\text{I}_2)$ (Figure S1 in Supplementary Materials) showed vibration peaks between 700 cm^{-1} and 1500 cm^{-1} , which can be attributed to the skeletal vibration of the phthalocyanine macrocycle [85]. The obtained $[(\text{Sb}^{\text{III}}\text{Pc})_2(\text{Sb}_2\text{I}_8)(\text{SbBr}_3)]$ crystals have limited solubility in methanol and ethanol and dissolve much better in pyridine, DMF, DMSO, toluene, benzene, and other aromatic solvents. Contact with concentrated inorganic acids, such as H_2SO_4 or HNO_3 , or their mixture or mixture with concentrated HCl leads to demetallation, resulting in the formation of metal-free phthalocyanine in the α -form [86] and appropriate salt.

3.2. Structural Characterization

The obtained antimony-phthalocyanine complex crystallizes in the centrosymmetric space group of the triclinic system. Refinement of the structure of the title compound (**1**) shows that both ionic parts of the crystal building blocks, i.e., in $(\text{SbPc})^+$ as well as in the $[(\text{Sb}_2\text{I}_8)(\text{SbBr}_3)]^{2-}$, contain the antimony in the same oxidation state (Sb^{3+}). The molecular structure of the asymmetric unit is illustrated in Figure 1.

Both independent $(\text{SbPc})^+$ units exhibit similar non-planar conformation, since the Sb^{3+} (ionic radius of about 0.90 \AA [69]) is larger than the equilibrium cavity size of the ring and cannot be accommodated without ring expansion; thus, the metal protrudes out of the Pc-cavity, forming a domed shape. Each of the positively charged atoms, Sb4 and Sb4B, of the cations $(\text{SbPc})^+$ is bound to four isoindole N atoms of Pc macrocycles with distances in the range from $2.146(8)$ to $2.206(8)\text{ \AA}$ (Table 2) and lies outside the plane defined by these N atoms, i.e., $0.992(1)$ and $0.994(1)\text{ \AA}$ for Sb4 and Sb4B, respectively. The optimized geometry of the $(\text{SbPc})^+$ unit performed by DFT calculations also show its non-planar conformation with the Sb atom displaced by 0.886 \AA out of N_4 -isoindole plane (See Table S1 in Supplementary Materials). The greater displacement of Sb(III) from the N_4 -plane in the crystal is caused by the interaction of the positively polarized Sb^{3+} center of $(\text{SbPc})^+$ with the $(\text{Sb}_6\text{I}_{16}\text{Br}_6)^{4-}$ counterion.

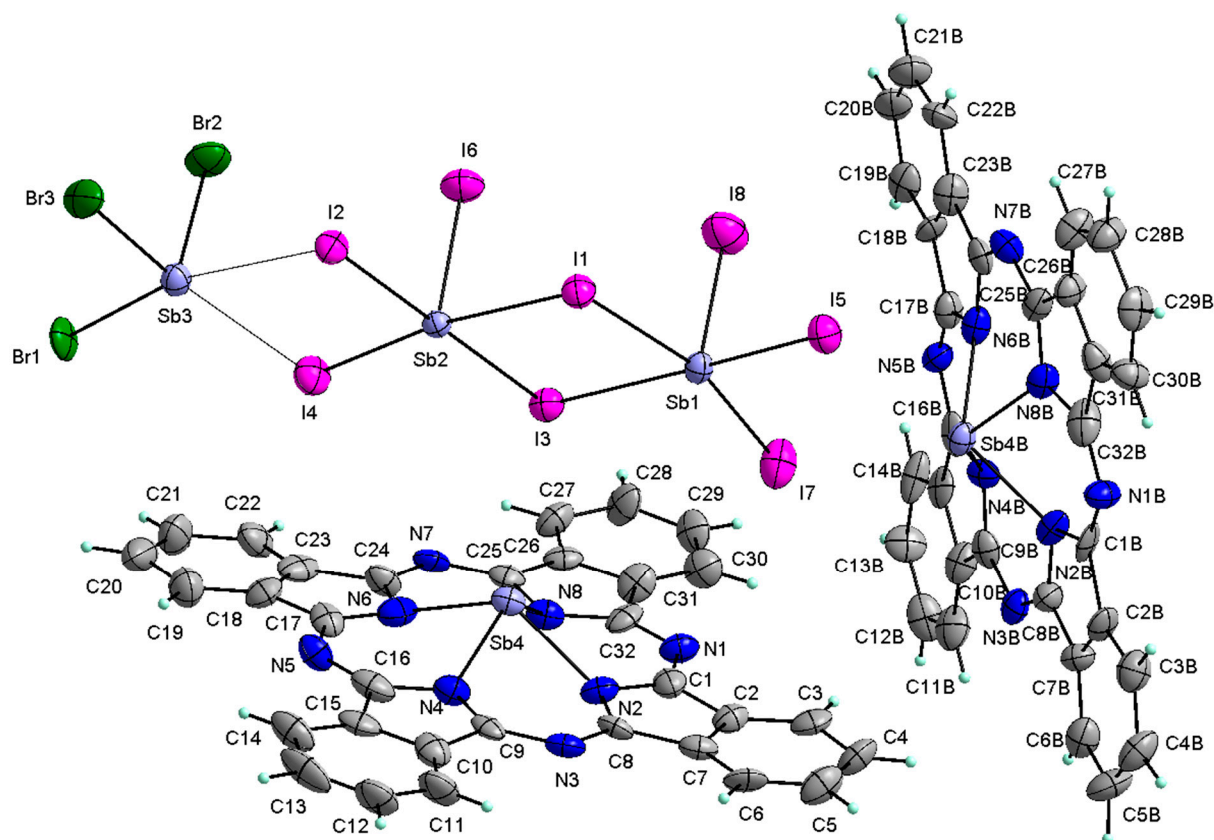


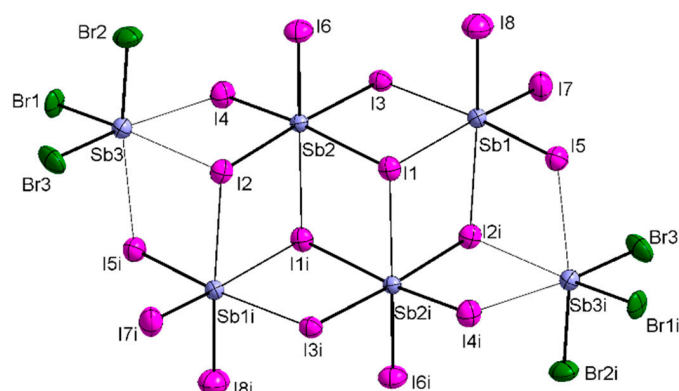
Figure 1. Asymmetric unit of **1** showing two independent $(\text{SbPc})^+$ units and $(\text{Sb}_3\text{I}_8\text{Br}_3)^{2-}$.

The anion of the complex consists of four distorted SbI_6 octahedra lined together by μ_2 and μ_3 bridging I atoms into a $(\text{Sb}_4\text{I}_{16})^{4-}$ anion that weakly interacts with two SbBr_3 molecules forming the centrosymmetric $(\text{Sb}_6\text{I}_{16}\text{Br}_6)^{4-}$ counterion complex (Figure 2). Generally, the Sb–I bond lengths fall into two groups, namely shorter Sb–I bonds with terminal I atoms and longer Sb–I bonds involving the bridging I atoms (Table 2). However, in the $(\text{Sb}_6\text{I}_{16}\text{Br}_6)^{4-}$ anion, two different bridging I atoms exist. Atoms I1 and I2 bridge three Sb atoms, while atoms I3, I4, and I5 bridge only two Sb atoms. The Sb–Br bonds with distances ranging from 2.5659(14) to 2.6888(12) Å are shorter, as expected, than the Sb–I bonds (Table 2) and correlate with their covalent or ionic radii of I and Br [87,88]. Looking in more detail at the differences between the Sb–I and Sb–Br bond lengths and at the coordination geometry around atoms Sb1, Sb2, and Sb3, it is clear the Sb1 and Sb2 atoms are coordinated to the six I atoms through forces of different strength, whereas Sb3 coordinates to three Br and the three I atoms. Atom Sb1 links two I atoms with relatively short Sb–I bonds, two I atoms with intermediate Sb–I values, and two I atoms with relatively long Sb–I bonds, the longest being the $\text{Sb1}^i\text{--I1}$ bond 3.4281(12) Å (Table 2).

The Sb2 atom in the coordination environment has one terminal I atom with the short Sb–I bond (2.7374(11) Å), two μ_2 -bridged, and three μ_3 -bridged I atoms with intermediate and longest Sb–I bonds (Table 2). The Sb3 links three Br atoms, all Br are terminal, with relatively short Sb–Br bond lengths, and the two μ_2 -bridged and one μ_3 -bridged I atoms with relatively long Sb–I bonds above 3.3 Å. Thus, the $[\text{Sb}_6\text{I}_{16}\text{Br}_6]^{4-}$ ion can be regarded as being composed of three symmetrically equivalent pairs of units, viz. $[\text{SbI}_5]^{2-}$, SbI_3 , and SbBr_3 units. However, the mutual orientation of the $[\text{SbI}_5]^{2-}$, SbI_3 , and SbBr_3 units related by an inversion center leads to the formation of an $[\text{Sb}_6\text{I}_{16}\text{Br}_6]^{4-}$ counter-ion in which all Sb atoms have distorted octahedral coordination environments (Figure 2).

Table 2. Selected bond lengths and angles (Å, °) in crystal of **1**.

(SbPc)⁺ Cations					
Sb4–N2	2.191(8)	Sb4B–N2B	2.202(7)		
Sb4–N4	2.178(8)	Sb4B–N4B	2.181(7)		
Sb4–N6	2.190(9)	Sb4B–N6B	2.206(8)		
Sb4–N8	2.206(8)	Sb4B–N8B	2.146(8)		
N2–Sb4–N4	78.0(3)	N2B–Sb4B–N4B	77.6(3)		
N4–Sb4–N6	79.4(3)	N4B–Sb4B–N6B	77.7(3)		
N6–Sb4–N8	77.5(3)	N6B–Sb4B–N8B	78.5(3)		
N2–Sb4–N8	77.7(3)	N2B–Sb4B–N8B	78.4(3)		
Deviation of Sb from N ₄ -plane	0.992(1)	Deviation of Sb from N ₄ -plane	0.994(1)		
(Sb₆I₁₆Br₆)^{4−} Anion					
Terminal Sb–I					
Sb1–I7	2.7668(13)	Sb1–I8	2.6965(12)	Sb2–I6	2.7374(11)
Bridged μ₂					
Sb1–I3	3.2329(11)	Sb2–I3	2.9833(13)	Sb1–I5	2.8744(11)
Sb3–I5 ⁱ	3.4481(10)	Sb2–I4	2.8302(10)	Sb3–I4	3.31901(10)
Bridged μ₃					
Sb1–I1	3.1765(14)	Sb2–I1	3.1856(11)	Sb2 ⁱ –I1	3.3610(10)
Sb2–I2	3.0061(13)	Sb1 ⁱ –I2	3.4281(12)	Sb3–I2	3.3531(11)
Terminal Sb–Br					
Sb3–Br1	2.6888(12)	Sb3–Br2	2.5659(14)	Sb3–Br3	2.6321(15)
I8–Sb1–I7	96.78(4)	I8–Sb1–I5	90.48(4)	I7–Sb1–I5	98.42(4)
I8–Sb1–I1	93.88(4)	I7–Sb1–I1	166.21(3)	I5–Sb1–I1	90.20(3)
I8–Sb1–I3	91.83(3)	I7–Sb1–I3	85.88(4)	I5–Sb1–I3	174.85(3)
I1–Sb1–I3	85.05(3)	I6–Sb2–I4	97.06(3)	I6–Sb2–I3	90.66(4)
I4–Sb2–I3	88.68(3)	I6–Sb2–I2	91.49(3)	I4–Sb2–I2	93.83(4)
I3–Sb2–I2	176.48(3)	I6–Sb2–I1	90.88(3)	I4–Sb2–I1	171.80(3)
I3–Sb2–I1	89.16(3)	I2–Sb2–I1	88.02(3)	Br2–Sb3–Br3	92.11(5)
Br2–Sb3–Br1	97.60(5)	Br3–Sb3–Br1	96.8(5)	Sb1–I1–Sb2	91.46(3)
Sb2–I3–Sb1	94.17(3)				
Short Contacts between (SbPc)⁺ Units and (Sb₆I₁₆Br₆)^{4−} Anion					
Sb4–I1 ⁱ	3.5083(13)	Sb4–I2 ⁱ	3.6471(13)	Sb4–I3	3.6115(14)
Sb4B–I5	3.6283(14)	Sb4B–I7	3.4969(11)	Sb4B–Br3 ⁱ	3.5941(18)

Symmetry Code: (*i*) $-x, -y, -z + 1$.**Figure 2.** View of the anionic unit of **1**.

A similar pattern concerning the Sb–I bond lengths is also observed in the [Sb₄I₁₆]^{4−} [59], [Sb₄I₁₄]^{2−} [62], and [Sb₆I₂₂]^{4−} [63] counter-ions of antimony(III)–phthalocyanine complexes. In the first complex, the [Sb₄I₁₆]^{4−} ion consists of four distorted SbI₆ octahedra, in the second, the [Sb₄I₁₄]^{2−} ion consists of two pairs of deformed SbI₆ octahedra and distorted square pyramidal SbI₅ polyhedra, while in the third, the [Sb₆I₂₂]^{4−} ion consists of six dis-

torted SbI_6 octahedra similar as in the present compound in which the Br atoms have been replaced by the I atoms. A similar metal-polyheterohalide anion can be found in the bismuth(III)-phthalocyanine derivative whose $[\text{Bi}_6\text{Cl}_{11}\text{I}_{11}]^{4-}$ anion consists of edge-shared distorted octahedra Bi_3Cl_3 [64].

In the crystal, there seems to be significant ionic attraction between the $(\text{SbPc})^+$ cations and $[\text{Sb}_6\text{I}_{16}\text{Br}_6]^{4-}$ complex counterions. The influence of the ionic attraction between the oppositely charged $(\text{SbPc})^+$ and $[\text{Sb}_6\text{I}_{16}\text{Br}_6]^{4-}$ ions is clearly manifested in the Sb–N(isoindole) coordination, leading to the molecular symmetry of the $(\text{SbPc})^+$ unit being close to C_s , rather than the D_{4v} symmetry that characterizes the conformation in solution. The basic packing unit includes two pairs of $(\text{SbPc})^+$ macrocycles associated by an inversion centre and an anionic $[\text{Sb}_6\text{I}_{16}\text{Br}_6]^{4-}$ complex; thus, each anion is surrounded by four $(\text{SbPc})^+$ cations (Figure 3).

Each of the two independent $(\text{SbPc})^+$ cations interact with the $[\text{Sb}_6\text{I}_{16}\text{Br}_6]^{4-}$ counterion in a slightly different manner. The Sb4 of $(\text{SbPc})^+$ interacts with three iodine atoms (I1, I2 and I3) while the Sb4B of $(\text{SbPc})^+$ interacts with two iodines (I5 and I7) and one bromine (Br3) with the contacts Sb–I and Sb–Br being much longer than the sum of the covalent radii of Sb (1.39 Å), I (1.40 Å) and Br (1.20 Å) [87] but shorter than the sum of the van der Waals radii Sb and I of ~ 4.3 Å or Sb and Br of ~ 4.1 Å [88]. The average Sb–I distance of 3.578 Å and the Sb–Br distance of 3.5941(18) Å between the Sb of $(\text{SbPc})^+$ units and I or Br atoms of $[\text{Sb}_6\text{I}_{16}\text{Br}_6]^{4-}$ complex anion point that the interaction between $(\text{SbPc})^+$ units and $[\text{Sb}_6\text{I}_{16}\text{Br}_6]^{4-}$ anion is intermediate between ionic and covalent. The centrosymmetric $[(\text{SbPc})_4(\text{Sb}_6\text{I}_{16}\text{Br}_6)]$ aggregates related by translation in crystal form a stacking structure along the [100] and [111] directions with back-to-back oriented $(\text{SbPc})^+$ pairs (Figure 4).

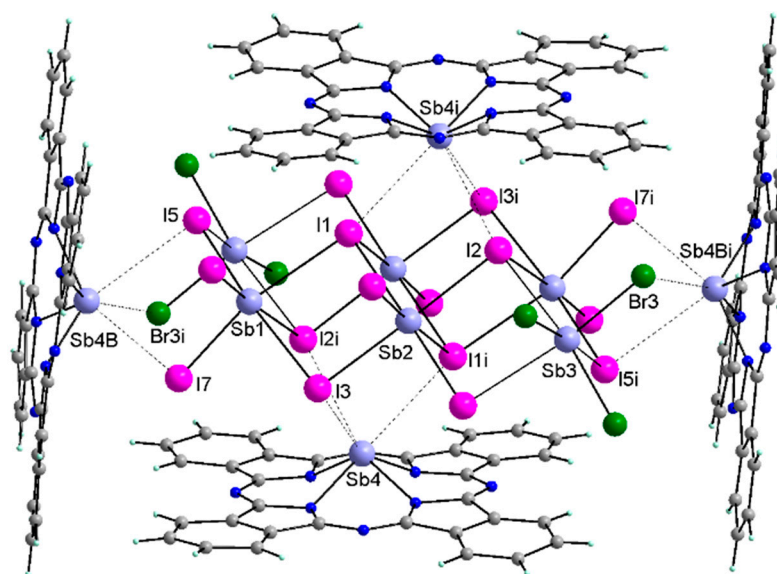


Figure 3. View of the anionic $[\text{Sb}_6\text{I}_{16}\text{Br}_6]^{4-}$ complex surrounded by four $(\text{SbPc})^+$ in the crystal of 1.

The interplanar $\text{N}_{4\text{-isoindole}}\text{--N}_{4\text{-isoindole}}$ distance within the stack is ~ 3.5 Å, which indicates an interaction between the non-planar $(\text{SbPc})^+$ macrocycles with an intermediate force. The π – π interaction and overlapping of the π clouds of $(\text{SbPc})^+$ macrocycles in the present crystal 1 is significantly lower compared to that found in the normal planar M(II)Pc structures. Decreasing of π – π interactions together with the ionic character of the $(\text{SbPc})^+$ and $(\text{Sb}_6\text{I}_{16}\text{Br}_6)^{4-}$ units result in improvement to its solubility as well as affects its optical spectroscopic properties.

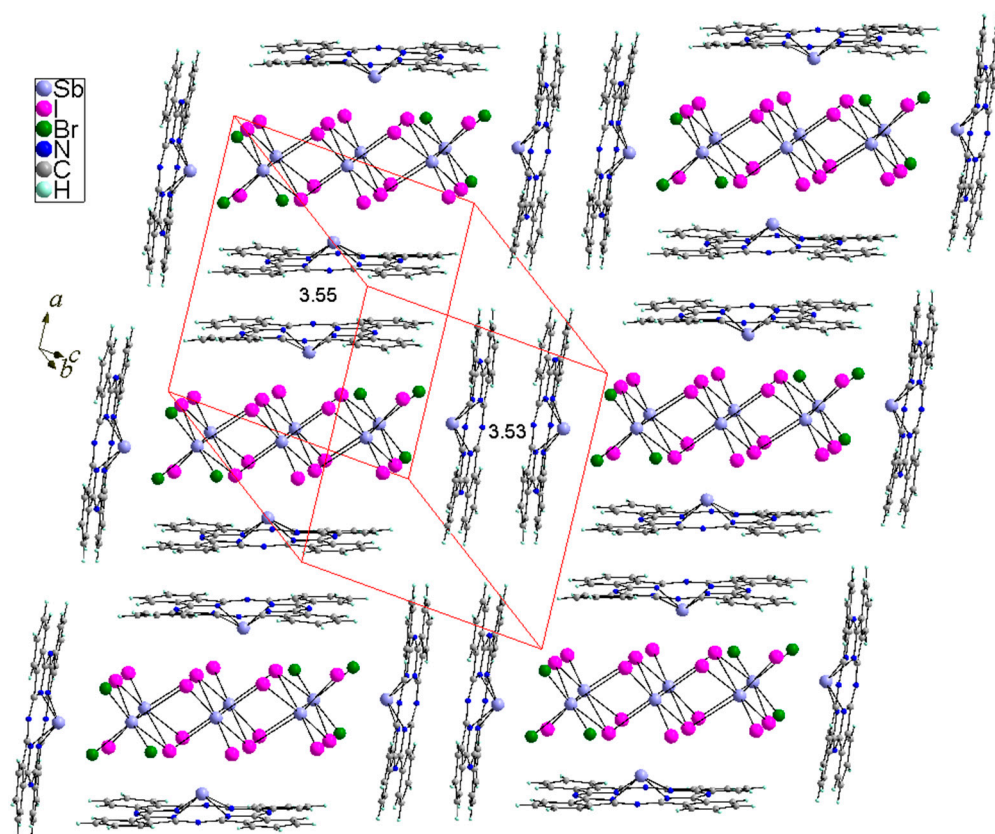


Figure 4. Packing of $[(\text{SbPc})_4(\text{Sb}_6\text{I}_{16}\text{Br}_6)]$ showing a stacking structure in **1**.

3.3. Hirshfeld Surface Analysis

To better understand the nature of the interactions between the components constituting the crystal **1**, the Hirshfeld surface analysis and the analysis of the 2D fingerprint plots were performed. The Hirshfeld surface (HS) analysis and the analysis of 2D fingerprint plots are good tools that not only allow for qualitative analysis of the intermolecular interactions in the crystals [89–92], but also allow for quantitative analysis, i.e., allow the percentage contribution to the HS surface resulting from particular types of interactions between building blocks of the crystal **1** to be calculated. The 3D Hirshfeld surfaces are mapped via the normalized contact distance (d_{norm}) relative to both (d_e) and (d_i) and the van der Waals radii of the atoms, where d_e is the distance from a point on the surface to the nearest nucleus outside the surface, and d_i is distance from a point on the surface to the nearest nucleus inside the surface and 2D-fingerprint plots of each units of crystal, i.e., both independent $(\text{SbPc})^+$ units and the $[\text{Sb}_6\text{I}_{16}\text{Br}_6]^{4-}$ counterion, and are shown in Figure 5. Where the atoms make intermolecular contacts closer than the sum of van der Waals radii, the contacts are highlighted in red on the HS mapped with the d_{norm} ; longer contacts are blue and the contacts around the sum of van der Waals radii are white. As can be seen from Figure 5, the HS analysis of both independent $(\text{SbPc})^+$ units in the crystal reveals that the $(\text{SbPc})^+$ units interact differently. The HS of both $(\text{SbPc})^+$ units exhibit that the dominant contacts are H–H interactions (dispersive forces) with a contribution of 36.7% and 45.0% in the HS of $(\text{SbPc})^+$ units containing the Sb4 and Sb4B, respectively. The interaction between the $(\text{SbPc})^+$ units with the $(\text{Sb}_6\text{I}_{16}\text{Br}_6)^{4-}$ counterion is manifested in the HS, and for the 2D-fingerprint plots that show the H–I contacts for the $(\text{SbPc})^+$ unit containing Sb4, the H–I contact contribution is greater (9.0%) than for the Sb4B unit (3.4%). However, in the HS of the second $(\text{SbPc})^+$ unit, the H–Br interactions with a contribution of ~4.5% are observed, but interactions of this type (H–Br) are absent in the HS for the first (SbPc) unit containing Sb4. Similar correlations as for H–I and H–Br are observed in the C–I and C–Br interactions in the HS of the $(\text{SbPc})^+$ units. The H–C/C–H and H–N/N–H interactions in the HS with

contributions of 17.3% and 5.9%, and 16.1% and 5.4%, respectively, are found in the SbPc units with Sb4 and Sb4B atoms, respectively. The contribution of the π - π interactions between the back-to-back-oriented pair of (SbPc)⁺ units, which correlate well with the C-C and C-N/N-C contacts in the HS of approximately 8.5% and 10.4% for (SbPc)₂ unit pairs containing Sb4 and Sb4B atoms, respectively, and is 2 ÷ 2.5 times smaller than in normal and planar metallophthalocyanine crystals in which these interactions reach about 22% [93].

The HS of the [Sb₆I₁₆Br₆]⁴⁻ unit shows small light-red areas resulting from the interaction of I-Sb and Br-Sb with the surrounding units (SbPc)⁺ with contributions of 6.8% and 1.4% in the HS. However, the main contribution to the HS results from the interactions of I-H and Br-H, which account for more than 50% of the HS area. The contribution in area of the HS of the (Sb₄I₁₆Br₆)⁴⁻ anion resulting from the I-C, Br-C, I-N, and Br-N interactions with a total share is about 40%. The deconvolution of the 2D-fingerprint plot illustrating the respective interactions for both independent (SbPc)⁺ units and for (Sb₄I₁₆Br₆)⁴⁻ counterion is shown in Figure S2 (in Supplementary Materials).

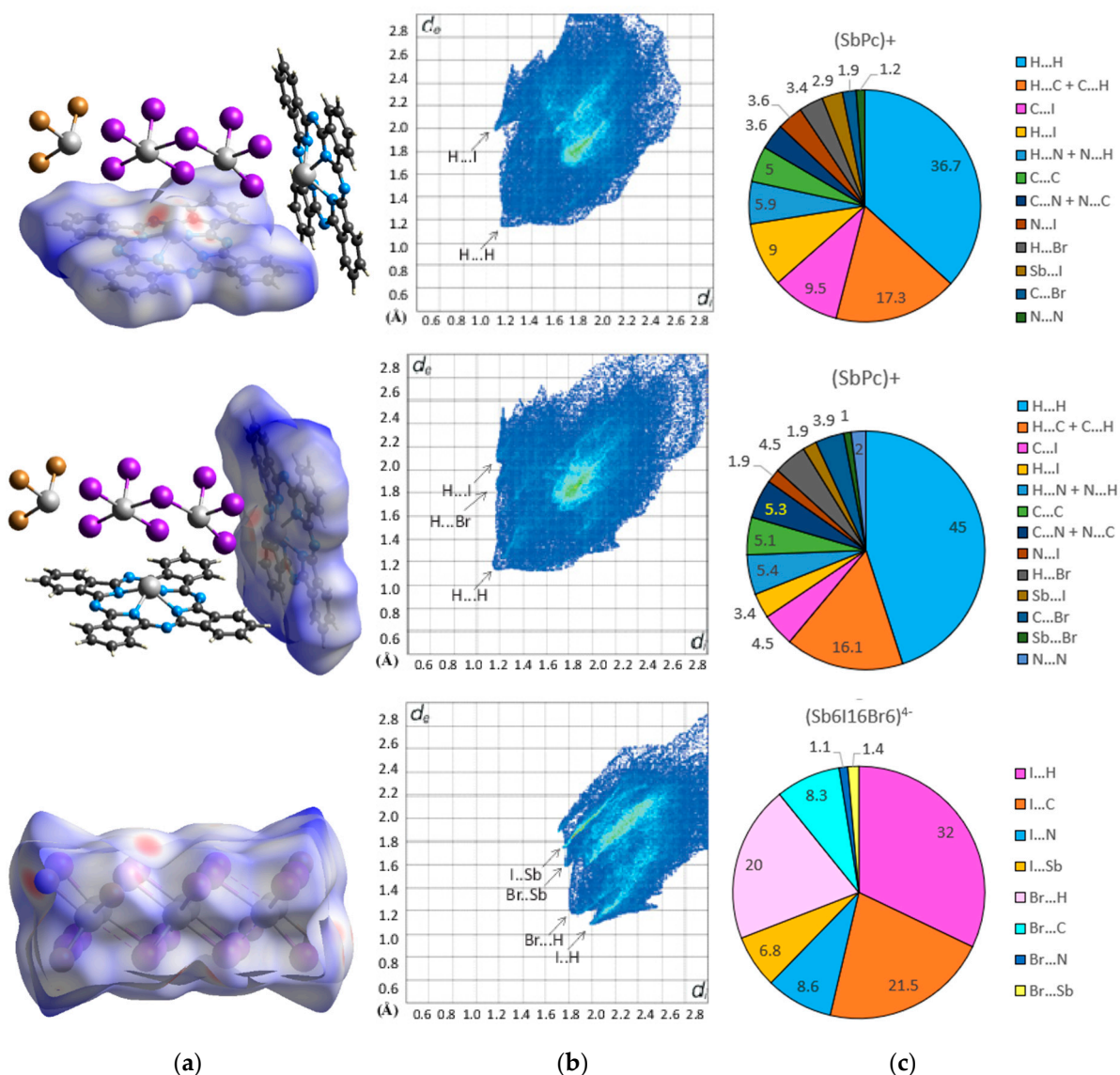


Figure 5. Hirshfeld surface (a) and the 2D-fingerprint plots (b) for each building units of the crystal 1 and (c) percentage contributions of the respective interactions in the HS.

3.4. UV–Vis Spectroscopy

To characterize the optical properties of the obtained antimony(III) phthalocyanine complex, $[(\text{SbPc})_4(\text{Sb}_6\text{I}_{16}\text{Br}_6)]$, the absorption UV–Vis electronic spectra were made in CH_2Cl_2 and toluene solutions (Figure 6). The ground state electronic absorption spectra of $[(\text{SbPc})_4(\text{Sb}_6\text{I}_{16}\text{Br}_6)]$ in CH_2Cl_2 and in toluene solutions show relatively sharp Q bands typical of unaggregated MPc complexes, as has been reported before for other antimony(III)–phthalocyanine derivatives [94,95]. The Q band in the spectrum of the $[(\text{SbPc})_4(\text{Sb}_6\text{I}_{16}\text{Br}_6)]$ complex in both solutions is broadened, and the half-width of this band is almost twice as wide as compared to the spectra of normal/flat M(II) Pc complexes [96–98], since the Sb(III) is larger than the equilibrium cavity size of the ring and cannot be accommodated without ring expansion; thus, the metal protrudes out of the cavity, forming a non-planar Sb(III) phthalocyanine complex. Thus, the symmetry of the $(\text{SbPc})^+$ complex unit in solution becomes D_{4v} symmetry that is lower than D_{4h} as for normal/planar MPc complexes in solutions [99]. Lowering of the symmetry of the $(\text{SbPc})^+$ allows for some so far forbidden transitions, and consequently, spectral splitting as well as a broadening is observed. The Q-band, an electronic transition from HOMO to LUMO of the phthalocyanine ligand in character, in the spectrum of the SbPc complex **1** in the CH_2Cl_2 solution is observed at ~ 725 nm ($\log \epsilon = 5.33$), and the Q band in the spectrum in toluene solution is red shifted to ~ 740 nm ($\log \epsilon = 5.35$), whereas for normal, planar and with D_{4h} symmetry of metal(II) phthalocyanines, the Q band is observed at almost the same wavelength (~ 670 nm) [100].

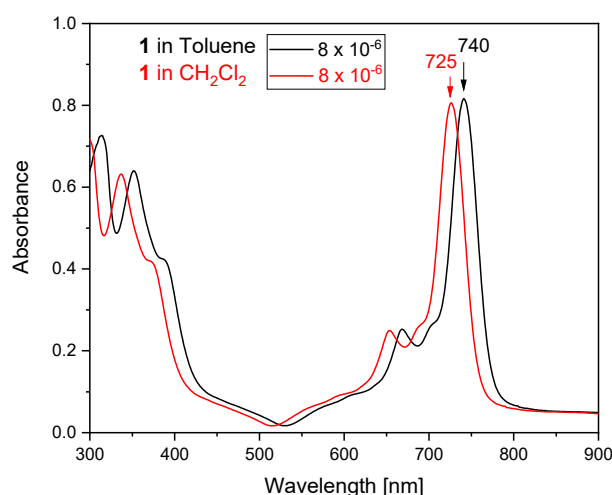


Figure 6. Electronic absorption spectra of antimony(III) phthalocyanine (**1**), $[(\text{SbPc})_4(\text{Sb}_6\text{I}_{16}\text{Br}_6)]$, in toluene (black) and CH_2Cl_2 (red) solutions.

The aggregation behavior of the investigated antimony(III)–phthalocyanine complex (**1**), $[(\text{SbPc})_4(\text{Sb}_6\text{I}_{16}\text{Br}_6)]$, was examined by varying the concentrations in both used solvents within the limits of the Beer–Lambert’s law. The aggregation of phthalocyanines, especially the planar metallophthalocyanines occurs in solution through a coplanar association that makes the conversion of a monomer to higher order complexes. However, this antimony(III) phthalocyanine complex, due to the non-planarity of the $(\text{SbPc})^+$ unit and the partially ionic character of the complex, is better soluble in the most organic common solvents. The aggregation behavior of the $[(\text{SbPc})_4(\text{Sb}_6\text{I}_{16}\text{Br}_6)]$ complex was investigated in CH_2Cl_2 and toluene solutions with concentrations between 8×10^{-6} mol/L and 10^{-6} mol/L. Both solvents are characterized by a non-zero dipole moment, $\mu = 1.60$ D and $\mu = 0.36$ D for CH_2Cl_2 and toluene, respectively [101]. The antimony(III) phthalocyanine complex (**1**) has minimum aggregation in both solvents, as illustrated in Figure 7. With an increase in concentration, the intensity of absorption of the Q-band increased linearly, with no new band and wavelength shifts observed, which clearly evidenced that the aggregate species was not observed.

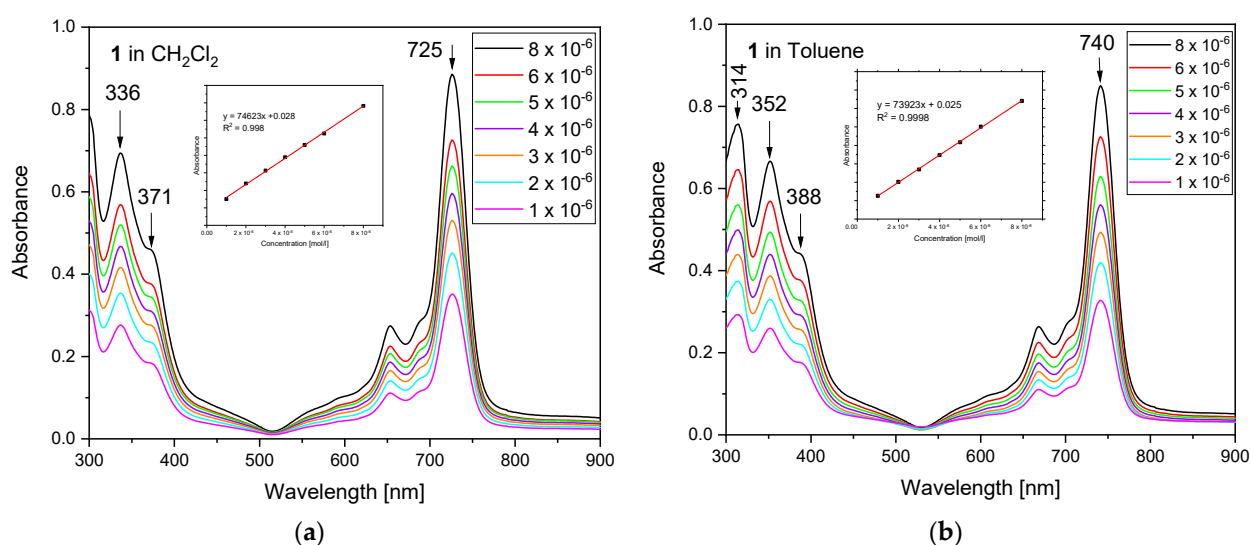


Figure 7. Optical absorption spectra of SbPc-complex 1 in CH_2Cl_2 (a) and in toluene (b) at various concentrations (8×10^{-6} – 1×10^{-6} mol/L).

The ability of $[(\text{SbPc})_4(\text{Sb}_6\text{I}_{16}\text{Br}_6)]$ to oxidize by H_2O_2 in a methanol solution was investigated. Hydrogen peroxide as an oxidant of metallophthalocyanines was often used. Therefore, for oxidation of $[(\text{SbPc})_4(\text{Sb}_6\text{I}_{16}\text{Br}_6)]$ dissolved in methanol (concentration of 5×10^{-6} mol/L) to $\text{Sb}^{\text{V}}\text{Pc}$ derivative the H_2O_2 was also used. The changes in the absorption spectrum in the range of the Q band (500–900 nm) during the oxidation process were monitored over time (Figure 8).

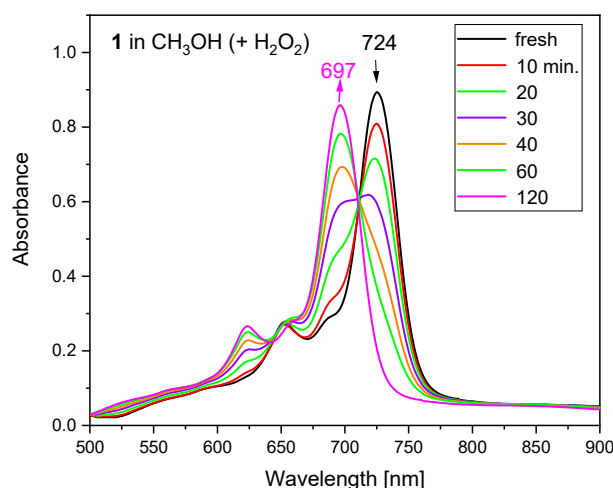


Figure 8. Spectral changes during the oxidation by H_2O_2 of 5×10^{-6} mol $[(\text{SbPc})_4(\text{Sb}_6\text{I}_{16}\text{Br}_6)]$ in methanol. The Q bands at 724 nm and 697 nm are characteristic for the Sb^{III} and for Sb^{V} phthalocyanines, respectively.

The Q band characteristic of $\text{Sb}^{\text{III}}\text{Pc}$ at 724 nm begins to decrease with the simultaneous appearance and increase in intensity of the Q band characteristic for $\text{Sb}^{\text{V}}\text{Pc}$ derivatives. Complete disappearance of the Q band from $(\text{Sb}^{\text{III}}\text{Pc})^+$ occurred after approximately 2 h. Oxidation of Sb^{3+} to Sb^{5+} is associated with a reduction of the ionic radius from 0.90 to 0.64 Å [69], with the result that the too large Sb^{3+} ion protruding from the ring plane in $(\text{Sb}^{\text{III}}\text{Pc})^+$ after oxidation to Sb^{5+} adapts to the size of the ring cavity. Thus, the Sb^{5+} lies in the plane of the Pc ring. The smaller size and higher electronegativity lead to increasing the conjugation of the Pc's HOMO with the metal 5 p_z orbital [102], which results in lower charge density and energy of the Pc's HOMO. The effect of this is the observed blue shifting

of spectral Q band positions (Figure 8). In the solution after oxidation of $(\text{Sb}^{\text{III}}\text{Pc})^+$ with D_{4v} symmetry by H_2O_2 , the $[\text{Sb}^{\text{V}}\text{Pc}(\text{OH})_2]^+$ complex with OH groups in the trans positions with approximately D_{4h} symmetry is formed. A quite similar correlation between the Q bands was observed during the oxidation of the complex $(\text{SbPc})(\text{I}_3) \cdot \frac{1}{2}\text{I}_2$ [68]. This Sb(V)-phthalocyanine complex, $[\text{Sb}^{\text{V}}\text{Pc}(\text{OH})_2]^+$, was also suggested by Knör [15], who studied the oxidation of $(\text{Sb}^{\text{III}}\text{Pc})\text{F}$ by hydrogen peroxide in an ethanol solution.

4. Conclusions

A new, low valence antimony–phthalocyanine complex under iodine vapor atmosphere, $[(\text{SbPc})_4(\text{Sb}_6\text{I}_{16}\text{Br}_6)]$ —(1), was obtained in the crystalline form. In the crystal, the $(\text{SbPc})^+$ unit is non-planar, since the Sb(III) is larger than the cavity size of the ring; thus, the metal protrudes out of the cavity, forming a saucer shape. The Hirshfeld surface analysis and the analysis of two-dimensional fingerprint plots show approximately 2.5 times lower π – π interaction between the partially overlapping and saucer-shaped phthalocyanine rings of $(\text{SbPc})^+$ units compared to normal, planar MPc's. This improves its solubility. In the CH_2Cl_2 solution, the Q band is observed at 725 nm, whereas in toluene solution this band is red shifted to 740 nm. Since the $[(\text{SbPc})_4(\text{Sb}_6\text{I}_{16}\text{Br}_6)]$ as a low valent metal of 15 main group phthalocyanine complex is similar to other $\text{Sb}^{\text{III}}\text{Pc}$ derivatives, it does not fluorescence; therefore, it can be used as precursor in obtaining (after oxidation) the high valent $\text{Sb}^{\text{V}}\text{Pc}$ complex that is similar to other Sb^{V} -phthalocyanine derivatives, showing the fluorescence excitation spectral. Oxidation of the complex $(\text{Sb}^{\text{III}}\text{Pc})^+$ with D_{4v} symmetry yields the $[\text{Sb}^{\text{V}}\text{Pc}(\text{OH})_2]^+$ complex with OH groups in the trans positions with approximately D_{4h} symmetry. It should also be noted that the $[(\text{SbPc})_4(\text{Sb}_6\text{I}_{16}\text{Br}_6)]$ before and after the oxidation to the $\text{Sb}^{\text{V}}\text{Pc}$ derivative show a characteristic UV–Vis absorption in the near-infrared range of 600–900 nm (i.e., in the therapeutic window), which should be intriguing from the point of view of potential use as an infrared cut-off filter for plasma displays, silicon photodiodes, solar cells, and charge-generating material as well as photosensitizers for semiconductor lasers or for PDT.

Supplementary Materials: The following supporting information can be downloaded at: <https://www.mdpi.com/article/10.3390/molecules27061839/s1>. Additional material contains the experimental IR spectrum of 1, full optimized parameters for $(\text{SbPc})^+$ unit and figures illustrating the deconvolution of the 2D-fingerprint plots for individual types of interactions in 1. CCDC No. 2131217 contains the supplementary crystallographic data for 1. These data can be obtained free of charge via <http://www.ccdc.cam.ac.uk/conts/retrieving.html> (accessed on 2 January 2022) or from the Cambridge Crystallographic Data Centre, 12 Union Road, Cambridge CB2 1EZ, UK; Fax: +44-1223-336-033; or email: deposit@ccdc.cam.ac.uk.

Author Contributions: Conceptualization, R.K. and J.J.; formal analysis, R.K. and J.J.; investigation, R.K. and J.J.; X-ray analysis, J.J.; writing—original draft preparation, R.K. and J.J.; writing—review and editing, R.K. and J.J. All authors have read and agreed to the published version of the manuscript.

Funding: This research received no external funding.

Institutional Review Board Statement: Not applicable.

Informed Consent Statement: Not applicable.

Acknowledgments: The authors would like to thank for the opportunity of making calculations with the Gaussian2016 program package in the Wrocław Center for Network and Supercomputing (<http://www.wcss.wroc.pl> (accessed on 2 January 2022)).

Conflicts of Interest: The authors declare no conflict of interest.

References

1. Herbst, W.; Hunger, K. *Industrial Organic Pigments: Production, Properties, Applications*; VCH: New York, NY, USA, 1993.
2. Gregory, P. Industrial Application of Phthalocyanines. *J. Porhyr. Phthalocyanines* **2000**, *4*, 432–437. [[CrossRef](#)]
3. Gregory, P. *High-Technology Applications of Organic Colorants*; CRC Press: Boca Raton, FL, USA, 1983.

4. Leznoff, C.C.; Lever, A.B.P. (Eds.) *Phthalocyanines: Properties and Applications*; VCH Publications: New York, NY, USA, 1989; Volume 1.
5. Leznoff, C.C.; Lever, A.B.P. (Eds.) *Phthalocyanines: Properties and Applications*; VCH Publications: New York, NY, USA, 1993; Volume 2.
6. Leznoff, C.C.; Lever, A.B.P. (Eds.) *Phthalocyanines: Properties and Applications*; VCH Publications: New York, NY, USA, 1996; Volume 3.
7. Leznoff, C.C.; Lever, A.B.P. (Eds.) *Phthalocyanines: Properties and Applications*; VCH Publications: New York, NY, USA, 1996; Volume 4.
8. Thomas, A. *Phthalocyanine Research and Applications*; CRS Press: Boca Raton, FL, USA, 1990.
9. Moser, F.H.; Thomas, A.L. *The Phthalocyanines*; CRC: Boca Raton, FL, USA, 1983.
10. Gouterman, M. Spectra of Porphyrins. *J. Mol. Spectrosc.* **1961**, *6*, 138–163. [[CrossRef](#)]
11. Falk, J.E. *Porphyrins and Metalloporphyrins*; Elsevier Pub. Co.: Amsterdam, The Netherlands; New York, NY, USA, 1964; p. 232.
12. Whalley, M. Conjugated macrocycles. Part XXXII. Absorption spectra of tetrazaporphyrins and phthalocyanines. Formation of pyridine salts. *J. Chem. Soc.* **1961**, 866–869. [[CrossRef](#)]
13. Barnett, G.H.; Hudson, M.F.; Smith, K.M. Concerning meso-tetraphenylporphyrin purification. *J. Chem. Soc. Perkin Trans. I* **1975**, *14*, 1401–1403. [[CrossRef](#)]
14. Ghani, F.; Kristen, J.; Riegler, H. Solubility Properties of Unsubstituted Metal Phthalocyanines in Different Types of Solvents. *J. Chem. Eng. Data* **2012**, *57*, 439–449. [[CrossRef](#)]
15. Knör, G. Synthesis and solution spectral properties of antimony(III) phthalocyanine and dihydroxoantimony(V) phthalocyanine complexes. *Inorg. Chem.* **1996**, *35*, 7916–7918. [[CrossRef](#)]
16. Modibane, D.K.; Nyokong, T. Synthesis, photophysical and photochemical properties of octa-substituted antimony phthalocyanines. *Polyhedron* **2009**, *28*, 479–484. [[CrossRef](#)]
17. Wright, Gas adsorption on phthalocyanines and its effects on electrical properties. *J. Prog. Surf. Sci.* **1989**, *31*, 1–60. [[CrossRef](#)]
18. Bassoul, P.; Toupance, T.; Simon, J. Semiconductivity and gas-sensing properties of crown-ether-substituted lutetium bisphthalocyanines. *Sens. Actuators B* **1995**, *26*, 150–152. [[CrossRef](#)]
19. Torre, G.; Vázquez, P.; Agulló-López, F.; Torres, T. Phthalocyanines and related compounds: Organic targets for nonlinear optical applications. *J. Mater. Chem.* **1998**, *8*, 1671–1683. [[CrossRef](#)]
20. Shirk, J.S.; Pong, R.G.S.; Flom, S.R.; Heckmann, H.; Hanack, M. Effect of Axial Substitution on the Optical Limiting Properties of Indium Phthalocyanines. *J. Phys. Chem. A* **2000**, *104*, 1438–1449. [[CrossRef](#)]
21. Torre, G.; Vázquez, P.; Lopez, F.A.; Torres, T. Role of structural factors in the nonlinear optical properties of phthalocyanines and related compounds. *Chem. Rev.* **2004**, *104*, 3723–3750. [[CrossRef](#)] [[PubMed](#)]
22. Gu, D.; Chen, Q.; Shu, J.; Tang, X.; Fuxi, G.; Sten, S.; Liu, K.; Xu, X. Optical recording performance of thin films of phthalocyanine compounds. *Thin Solid Films* **1995**, *275*, 88–93. [[CrossRef](#)]
23. Meng, Z.; Aykanat, A.; Mirica, K.A. Welding Metallophthalocyanines into Bimetallic Molecular Meshes for Ultrasensitive, Low-Power Chemiresistive Detection of Gases. *J. Am. Chem. Soc.* **2019**, *141*, 2046–2053. [[CrossRef](#)] [[PubMed](#)]
24. Choy, C.H.W.; Liang, Y.J.; Hui, K.N.; Fong, H.H. Improving the efficiency of OLEDs by utilizing metallophthalocyanines. In *Proceedings of the Optics and Photonics 2005*, San Diego, CA, USA, 31 July–4 August 2005; Volume 5937. [[CrossRef](#)]
25. Pearson, A.J.; Plint, T.; Jones, S.T.E.; Lessard, B.H.; Credgington, D.; Bender, T.P.; Greenham, N.C. Silicon phthalocyanines as dopant red emitters for efficient solution processed OLEDs. *J. Mater. Chem. C* **2017**, *5*, 12688–12698. [[CrossRef](#)]
26. Bharati, M.S.S.; Bhattacharya, S.; Krishna, J.V.S.; Giribabu, L.; Rao, S.V. Femtosecond, broadband nonlinear optical studies of a zinc porphyrin and zinc phthalocyanine. *Opt. Laser Technol.* **2018**, *108*, 418–425. [[CrossRef](#)]
27. Bhattacharya, S.; Reddy, G.; Paul, S.; Hossain, S.S.; Raavi, S.S.K.; Giribabu, L.; Samanta, A.; Soma, V.R. Comparative photophysical and femtosecond third-order nonlinear optical properties of novel imidazole substituted metal phthalocyanines. *Dyes Pigments* **2021**, *184*, 108791. [[CrossRef](#)]
28. Ben-Hur, E.; Chan, W.-S. Phthalocyanines in Photobiology and Their Medical Applications. In *The Porphyrins Handbook*; Kadish, K.M., Smith, K.M., Guillard, R., Eds.; Academic Press: Boston, FL, USA, 2003; Volume 19, pp. 1–35.
29. Bonnett, R. *Chemical Aspects of Photodynamic Therapy*; Gordon and Breach Science Publishers: Amsterdam, The Netherlands, 2000.
30. Moreira, L.M.; Vieira dos Santos, F.; Pereira Lyon, J.; Maftoum-Costa, M.; Pacheco-Soares, C.; Soares da Silva, N. Photodynamic Therapy: Porphyrins and Phthalocyanines as Photosensitizers. *Aust. J. Chem.* **2008**, *61*, 741–754. [[CrossRef](#)]
31. Lopez, T.; Ortiz, E.; Alvarez, M.; Navarrete, J.; Odriozola, A.; Martinez-Ortega, F.; Páez-Mozo, E.A.; Escobar, P.; Espinoza, K.A.; Rivero, I.A. Study of the stabilization of zinc phthalocyanine in sol-gel TiO₂ for photodynamic therapy applications. *Nanomed. Nanotechnol. Biol. Med.* **2010**, *6*, 777–785. [[CrossRef](#)]
32. Mfouo-Tynga, I.; Houreld, N.N.; Abrahamse, H. Induced Cell Death Pathway Post Photodynamic Therapy Using a Metallophthalocyanine Photosensitizer in Breast Cancer Cells. *Photomed. Laser Surg.* **2014**, *32*, 205–211. [[CrossRef](#)]
33. Neagu, M.; Constantin, C.; Tampa, M.; Matei, C.; Lupu, A.; Manole, E.; Ion, R.M.; Fenga, C.; Tsatsakis, A.M. Toxicological and efficacy assessment of post-transition metal 9indium phthalocyanine for photodynamic therapy in neuroblastoma. *Oncotarget* **2016**, *7*, 69718–69732. [[CrossRef](#)] [[PubMed](#)]

34. Oluwole, D.O.; Manoto, S.L.; Malabi, R.; Maphanga, C.; Ombinda-Lemboumba, S.; Mthunzi-Kufa, P.; Nyokong, T. Evaluation of the photophysical properties and photodynamic therapy activity of nanoconjugates of zinc phthalocyanine linked to glutathione capped Au and Au₃Ag₁ nanoparticles. *Dyes Pigments* **2018**, *150*, 139–150. [[CrossRef](#)]
35. Dube, E.; Oluwole, D.O.; Prinsloo, E.; Nyokong, T. A gold-chitosan composite with low symmetry zinc phthalocyanine for enhanced singlet oxygen generation and improved photodynamic therapy activity. *New J. Chem.* **2018**, *42*, 10214–10225. [[CrossRef](#)]
36. Dumoulin, F.; Durmus, M.; Ahsen, V.; Nyokong, T. Synthetic pathways to water-soluble phthalocyanines and close analogs. *Coord. Chem. Rev.* **2010**, *254*, 2792–2848. [[CrossRef](#)]
37. Terekhov, D.S.; Nolan, K.J.M.; McArthur, C.R.; Leznoff, C.C. Synthesis of 2,3,9,10,16,17,23,24-Octaalkynylphthalocyanines and the Effects of Concentration and Temperature on Their ¹H NMR Spectra. *J. Org. Chem.* **1996**, *61*, 3034–3040. [[CrossRef](#)]
38. Isago, H.; Leznoff, C.C.; Ryan, M.F.; Metcalfe, R.A.; Davids, R.; Lever, A.B.P. Aggregation Effects on Electrochemical and Spectroelectrochemical Properties of [2,3,9,10,16,17,23,24-Octa(3,3-dimethyl-1-butynyl)phthalocyaninato]cobalt(II) Complex. *Bull. Chem. Soc. Jpn.* **1998**, *71*, 1039–1047. [[CrossRef](#)]
39. Isago, H.; Terekhov, D.; Leznoff, C.C. Synthesis and NMR Studies of a Single Isomer of an Alkynyl Substituted Binuclear Phthalocyanine. *J. Porphyrins Phthalocyanines* **1997**, *1*, 135–140. [[CrossRef](#)]
40. Würthner, F. (Ed.) *Supramolecular Dye Chemistry*; Springer: Berlin/Heidelberg, Germany, 2005.
41. Menzel, E.R.; Rieckhoff, K.E.; Voigt, E.M. Dynamics of the triplet state of phthalocyanine complexes of the platinum metals in zero field. *J. Chem. Phys.* **1973**, *58*, 5726–5734. [[CrossRef](#)]
42. Hanack, M.; Schneider, T.; Barthel, M.; Shirk, J.S.; Flom, S.R.; Pong, R.G.S. Indium phthalocyanines and naphthalocyanines for optical limiting. *Coord. Chem. Rev.* **2001**, *219*, 235–258. [[CrossRef](#)]
43. Liu, Y.H.; Benassy, M.-F.; Chojnacki, S.; D'Souza, F.; Barbour, T.; Belcher, W.J.; Brothers, P.J.; Kadish, K.M. Electrochemical and Spectroelectrochemical Investigations of [(TpTP)MvL₂]+Cl⁻ Where TpTP is the Dianion of Tetra-p-tolyporphrin, M = P or Sb, and L = Cl⁻ or OCH₃⁻. *Inorg. Chem.* **1994**, *33*, 4480–4484. [[CrossRef](#)]
44. Yamamoto, Y.; Akiba, K.-y. The chemistry of Group 15 element porphyrins bearing element—Carbon bonds: Synthesis and properties. *J. Organomet. Chem.* **2000**, *611*, 200–209. [[CrossRef](#)]
45. Kadish, K.M.; Van Caemelbecke, E.; Royal, G. Electrochemistry of Metalloporphyrins in Nonaqueous Media. In *The Porphyrin Handbook*; Kadish, K.M., Smith, K.M., Guillard, R., Eds.; Academic Press: San Diego, CA, USA, 2000; Volume 8, pp. 83–87.
46. Satoh, W.; Masumoto, S.; Yamamoto, Y.; Akiba, K. Synthesis and properties of group 15 element porphyrin peroxides. *Heteroat. Chem.* **2001**, *12*, 431–443. [[CrossRef](#)]
47. Brothres, P.J. Recent developments in the coordination chemistry of porphyrin complexes containing non-metallic and semi-metallic elements. *J. Porphyr. Phthalocyanines* **2002**, *6*, 259–267. [[CrossRef](#)]
48. Isago, H.; Kagaya, Y. Syntheses and Characterization of Bromo- and Chloro(phthalocyaninato)bismuth(III) Complexes. *Bull. Chem. Soc. Jpn.* **1994**, *67*, 383–389. [[CrossRef](#)]
49. Isago, H.; Kagaya, Y. Spectroscopic Properties of One-Electron-Reduced Species of Dichloro(phthalocyaninato)antimony(V) cation. *Bull. Chem. Soc. Jpn.* **1996**, *69*, 1281–1288. [[CrossRef](#)]
50. Isago, H.; Kagaya, Y.; Nakajima, S.-I. Spectral Properties of Nonaggregative Antimony(V) Phthalocyanine and Its Film as a Novel Near-Infrared Absorber. *Chem. Lett.* **2003**, *32*, 112–113. [[CrossRef](#)]
51. Isago, H.; Miura, K.; Kanesato, M. Unexpected photo-initiated oxidation of antimony in (tetra-tert-butyl)phthalocyaninatoantimony(III) complex in the presence of singlet oxygen acceptors. *J. Photochem. Photobiol. A Chem.* **2008**, *197*, 313–320. [[CrossRef](#)]
52. Kubiak, R.; Razik, M. (Phthalocyaninato)antimony Iodide. *Acta Cryst. C* **1998**, *54*, 483–485. [[CrossRef](#)]
53. Kubiak, R.; Janczak, J.; Razik, M. Synthesis and X-ray characterization of phthalocyaninato(2-)antimony(III) triiodide. *Inorg. Chim. Acta* **1999**, *293*, 155–159. [[CrossRef](#)]
54. Janczak, J.; Kubiak, R.; Jezierski, A. Mixed-Valence, Disordered Structures and Characterization of Iodine-doped Phthalocyanines: [YbPc₂]I₂ and [(AsPc)₂]. *Inorg. Chem.* **1999**, *38*, 2043–2049. [[CrossRef](#)]
55. Janczak, J.; Kubiak, R.; Richter, J.; Fuess, H. Bismuth triple-decker phthalocyanine: Synthesis and structure. *Polyhedron* **1999**, *18*, 2775–2780. [[CrossRef](#)]
56. Kubiak, R.; Ejsmont, K. Crystal structure of a novel bismuth phthalocyanine-bismuth iodide complex. *J. Mol. Struct.* **1999**, *474*, 257–282. [[CrossRef](#)]
57. Hückstüdt, H.; Tutass, A.; Göldner, M.; Cornelissen, U.; Homborg, H. Conformational Heterogeneity in Diphthalocyaninato(2-)metalates(III) of Sc, Y, In, Sb, Bi, La, Ce, Pr and Sm. *Z. Anorg. Allg. Chem.* **2001**, *627*, 485–497. [[CrossRef](#)]
58. Janczak, J.; Kubiak, R. [Phthalocyaninato(2-)]antimony(III) chloride. *Acta Cryst. C* **2001**, *57*, 55–57. [[CrossRef](#)] [[PubMed](#)]
59. Janczak, J.; Idemori, Y.M. Tetrakis[phthalocyaninato(2-)antimony(III)] hexadecaiodotetraantimony(III). *Acta Cryst. C* **2002**, *58*, m23–m25. [[CrossRef](#)] [[PubMed](#)]
60. Janczak, J.; Idemori, Y.M. {Phthalocyaninato(2-)}arsenic(III) triiodide. *Acta Cryst. E* **2002**, *58*, m36–m38. [[CrossRef](#)]
61. Janczak, J.; Kubiak, R. Bis{[phthalocyaninato(2-)]arsenic(III)} tetradecaiodotetraarsenic(III). *Acta Cryst. C* **2003**, *59*, m70–m72. [[CrossRef](#)]
62. Perpetuo, G.J.; Janczak, J. Bis{[phthalocyaninato(2-)]antimony(III)} tetradecaiodotetraantimonate(III). *Acta Cryst. E* **2005**, *61*, m2003–m2005. [[CrossRef](#)]
63. Janczak, J.; Perpetuo, G.J. Tetrakis[phthalocyaninato(2-)antimony(III)] docosaiohexaantimony(III). *Acta Cryst. C* **2006**, *62*, m323–m326. [[CrossRef](#)]

64. Janczak, J. Synthesis and characterization of bismuth(III) phthalocyaninate complex: $[\text{BiPc}]_4[\text{Bi}_6\text{I}_{11}\text{Cl}_{11}]$. *J. Mol. Struct.* **2010**, *905*, 125–130. [[CrossRef](#)]
65. Kagaya, Y.; Isago, H. Facile Reduction of Dichloro(phthalocyaninato)antimony(V) Cation. *Chem. Lett.* **1994**, *23*, 1957–1960. [[CrossRef](#)]
66. Isago, H.; Kagaya, Y. Facile antimony(V/III) interconversion in phthalocyanine complexes. *Chem. Lett.* **2006**, *35*, 8–9. [[CrossRef](#)]
67. Kagaya, Y.; Isago, H. Synthesis of Dichloro(phthalocyaninato)antimony(V) Perchlorate, Tetrafluoroborate, and hexafluorophosphate and Electrochemical Reinvestigation on the New Complex Salts. *Bull. Chem. Soc. Jpn.* **1997**, *70*, 2179–2185. [[CrossRef](#)]
68. Janczak, J. The synthesis, structure and spectral properties of antimony(III) phthalocyanine obtained under iodine vapor atmosphere: $(\text{Sb}^{\text{III}}\text{Pc})(\text{I}_3) \cdot \frac{1}{2}(\text{I}_2)$. *Inorg. Chim. Acta* **2022**, *532*, 120758. [[CrossRef](#)]
69. Shannon, R.D. Revised effective ionic radii and systematic studies of interatomic distances in halides and chalcogenides. *Acta Cryst. A* **1976**, *32*, 751–767. [[CrossRef](#)]
70. Yan, S.; Jin, L.; Sun, H. ^{51}Sb antimony in medicine. In *Metallotherapeutic Drugs and Metal-Based Diagnostic Agents: The Use of Metals in Medicine*; Gielen, M., Tiekink, E.R.T., Eds.; John Wiley & Sons, Ltd.: Hoboken, NJ, USA, 2005.
71. Carter, K.C.; Hutchinson, S.; Boitelle, A.; Murray, H.W.; Sundar, S.; Mullen, A.B. Sodium stibogluconate resistance in *Leishmania donovani* correlates with greater tolerance to macrophage antileishmanial responses and trivalent antimony therapy. *Parasitology* **2005**, *131*, 747–757. [[CrossRef](#)]
72. Mandal, S.; Maharjan, M.; Singh, S.; Chatterjee, M.; Madhubala, R. Assessing aquaglyceroporin gene status and expression profile in antimony-susceptible and resistant clinical isolates of *Leishmania donovani* from India. *J. Antimicrob. Chemother.* **2010**, *65*, 496–507. [[CrossRef](#)]
73. Hadjikakou, S.K.; Ozturk, I.I.; Banti, C.N.; Kourkoumelis, N.; Hadjiliadis, N. Recent advances on antimony(III/V) compounds with potential activity against tumour cells. *J. Inorg. Biochem.* **2015**, *153*, 293–305. [[CrossRef](#)]
74. Maes, L.; Beyers, J.; Mondelaers, A.; Van den Kerkhof, M.; Eberhardt, E.; Caljon, G.; Hendrickx, S. In vitro ‘time-to-kill’ assay to assess the cidal activity dynamics of current reference drugs against *Leishmania donovani* and *Leishmania infantum*. *J. Antimicrob. Chemother.* **2017**, *72*, 428–430. [[CrossRef](#)]
75. Kubiak, R.; Janczak, J. A simple, novel method for the preparation of metallophthalocyanines. *J. Alloys Compd.* **1993**, *200*, L7–L8. [[CrossRef](#)]
76. *CrysAlis CCD and CrysAlis Red 1.171.38.43*; Rigaku Oxford Diffraction: Yaernaton, UK, 2015.
77. Sheldrick, G.M. SHELXT—Integrated space-group and crystal structure determination. *Acta Cryst. A* **2015**, *71*, 3–8. [[CrossRef](#)] [[PubMed](#)]
78. Sheldrick, G.M. Crystal structure refinement with SHELXL. *Acta Cryst. C* **2015**, *71*, 3–8. [[CrossRef](#)] [[PubMed](#)]
79. Brandenburg, K.; Putz, H. *DIAMOND Version 3.0*; Crystal Impact GbR: Bonn, Germany, 2006.
80. Wolff, S.K.; Grimwood, D.J.; MacKinnon, J.J.; Turner, M.J.; Jayatilaka, D. *Spackman, Crystal Explorer ver. 3.1*; University of Western Australia: Perth, Australia, 2013.
81. Frisch, M.J.; Trucks, G.W.; Schlegel, H.B.; Scuseria, G.E.; Robb, M.A.; Cheeseman, J.R.; Scalmani, G.; Barone, V.; Mennucci, B.; Petersson, G.A.; et al. *Gaussian16, Revision B.01*; Gaussian, Inc.: Wallingford, CT, USA, 2016.
82. Janczak, J.; Kubiak, R. Tris(2-cyanophenyl)-1,3,5-triazine: A By-product of Metallophthalocyanine Synthesis. *Acta Chem. Scand.* **1999**, *53*, 602–610. [[CrossRef](#)]
83. Barraclough, C.G.; Bissett, H.; Pitman, P.; Thustlethwaite, P.J. The infrared, Raman and ultraviolet spectra of phthalonitrile, terephthalonitrile and 2,6-dichlorobenzonitrile. *Aust. J. Chem.* **1977**, *30*, 753–765. [[CrossRef](#)]
84. Ogunsipe, A.; Opeolu, S. Synthesis, Characterization and Photostability Studies on Aluminium Phthalocyanine Chloride. *Chem. Res. J.* **2020**, *5*, 136–143.
85. Shurvell, H.F.; Pinzuti, L. Sur les spectres infraeouges des phthalocyanines. *Can. J. Chem.* **1966**, *44*, 125–136. [[CrossRef](#)]
86. Janczak, J. Comment on polymorphic forms of metal-free phthalocyanine. The refinement of the crystal structure of $\alpha\text{-H}_2\text{Pc}$ at 160 K. *Pol. J. Chem.* **2000**, *74*, 157–162.
87. Cordero, B.; Gómez, V.; Platero-Prats, A.E.; Revés, M.; Echeverría, J.; Cremades, E.; Barragán, F.; Alvarez, S. Covalent radii revisited. *Dalton Trans.* **2008**, *21*, 2832–2838. [[CrossRef](#)]
88. Batsanov, S.S. Van der Waals Radii of Elements. *Inorg. Mater.* **2001**, *37*, 871–885, Translated from *Neorganicheskie Materialy* 2001, *37*, 1031–1046. [[CrossRef](#)]
89. Spackman, M.A.; Jayatilaka, D. Hirshfeld surface analysis. *CrystEngComm* **2009**, *11*, 19–32. [[CrossRef](#)]
90. McKinnon, J.J.; Spackman, M.A.; Mitchell, A.S. Novel tools for visualizing and exploring intermolecular interactions in molecular crystals. *Acta Cryst. B* **2004**, *60*, 627–668. [[CrossRef](#)] [[PubMed](#)]
91. McKinnon, J.J.; Mitchell, A.S.; Spackman, M.A. Hirshfeld surfaces: A new tool for visualising and exploring molecular crystals. *Chem. Eur. J.* **1998**, *4*, 2136–2141. [[CrossRef](#)]
92. McKinnon, J.J.; Jayatilaka, D.; Spackman, M.A. Towards quantitative analysis of intermolecular interactions with Hirshfeld surfaces. *Chem. Commun.* **2007**, *37*, 3814–3816. [[CrossRef](#)] [[PubMed](#)]
93. Janczak, J. Coordination properties of diethylenetriamine in relation to zinc phthalocyanine. *Polyhedron* **2020**, *178*, 114313. [[CrossRef](#)]
94. Isago, H. Spectral properties of a novel antimony(III)-phthalocyanine complex that behaves like J-aggregates in non-aqueous media. *Chem. Commun.* **2003**, *15*, 1864–1865. [[CrossRef](#)]

95. Zahir, M.H.; Kagaya, Y.; Isago, H.; Furubayashi, T. Preparation of phthalocyanine(3-) species as bulk material by reduction of the dichloro(phthalocyaninato)antimony(V) complex cation. *Inorg. Chim. Acta* **2004**, *357*, 2755–2758. [[CrossRef](#)]
96. Bayo, K.; Mossoyan, J.C.; Ouedrago, G.V. Preparation and analysis by UV-Vis of zinc phthalocyanine complexes. *Spectrochim. Acta A* **2004**, *60*, 653–657. [[CrossRef](#)]
97. Staicu, A.; Pascu, A.; Nuta, A.; Sorescu, A.; Raditoiu, V.; Pascu, M.L. Studies about phthalocyanine photosensitizers to be used in photodynamic therapy. *Rom. Rep. Phys.* **2013**, *65*, 1032–1051.
98. Zhang, X.-F.; Guo, W. Imidazole functionalized magnesium phthalocyanine photosensitizer: Modified photophysics, singlet oxygen generation and photooxidation mechanism. *J. Phys. Chem. A* **2012**, *116*, 7651–7657. [[CrossRef](#)]
99. Tackley, D.R.; Dent, G.; Smith, W.E. Phthalocyanines: Structure and vibrations. *Phys. Chem. Chem. Phys.* **2001**, *3*, 1419–1426. [[CrossRef](#)]
100. Stillman, M.J.; Nyokong, T. Nonlinear Optical Properties of Phthalocyanines. In *Phthalocyanines, Properties and Applications*; Lever, A.B.P., Leznoff, C.C., Eds.; VCH: New York, NY, USA, 1989; Volume 1, Chapter 3.
101. Li, C.-P.; Du, M. Role of solvents in coordination supramolecular systems. *Chem. Commun.* **2011**, *47*, 5958–5972. [[CrossRef](#)] [[PubMed](#)]
102. Shelnutz, J.A. Correlation between metal stability, charge transfer, and Raman frequencies in metalloporphyrins and their π - π complexes. *J. Am. Chem. Soc.* **1983**, *105*, 774–778. [[CrossRef](#)]